Iraqi Journal of Physics, 2024 *Vol. 22, No. 2, PP. 90-103*
https://doi.org/10.30723/ijp.v22i2.1213
P-ISSN: 2070-4003
E-ISSN: 2664-5548

Corrosion Protection Performance of PACC and PACC-Metal Oxides Nanocomposites Electropolymerized Coating of Low Carbon Steel

Zainab A. Hussain[1a]* and Khulood A. Saleh[1b]
[1]*Department of Chemistry, College of Science, University of Baghdad, Baghdad, Iraq*
[b]*E-mail: khulood_abid@yahoo.com*
[a*]*Corresponding author: zainabalaa@yamil.com*

Abstract

In the current study, a novel conductive polymer poly 6-((4 acetylphenyl) carbamoyl) cyclohex-3-ene-1-carboxylic acid (PACC) was created by polymerized 6-((4 acetylphenyl) carbamoyl) cyclohex-3-ene-1-carboxylic acid (ACC) monomer using the electropolymerization process. The resulting polymer was characterized using Fourier transform Infrared spectroscopy (FTIR). The ability of this polymer to protect the alloy from corrosion was studied at temperatures ranging between 298 and 328 K. The ability of these coatings to stop corrosion on the surface was assessed by measuring the corrosion potential (E_{corr}) and the corrosion current (i_{corr}) using a potentiostat. Adding nanoscale metal oxides (zirconium dioxide (ZrO2) and magnesium oxides (MgO)) enhanced the efficiency of this polymeric coating. The protection efficiency of the polymer alone was 77.5%; this efficiency increased to 85.0% and 99.7% in the presence of nano ZrO_2 and MgO, respectively. Kinetic and thermodynamic parameters (E_a, H, and S) were calculated for uncoated and coated LCS. An atomic force microscope (AFM) studied the coating surface morphology. Electrochemical impedance spectroscopy (EIS) was used to evaluate the coating resistance.

Article Info.

Keywords:
Corrosion Protection, Conducting Polymers, Electropolymerization, PACC, Tafel.

Article history:
Received: Oct. 24, 2023
Revised: Apr. 15, 2024
Accepted: Apr. 27, 2024
Published: Jun. 01, 2024

1. Introduction

Steel is one of the materials needed in most industrial facilities because of its beneficial characteristics, like great durability, malleability, mechanical strength, etc. [1, 2]. The longevity of mild steel in most industrial installations is severely hampered by its exposure to adverse environmental factors and harsh chemicals (such as salts, aggressive chemicals, etc.). This is because it is quite likely that such circumstances lead to the beginning of the metal's electrochemical breakdown through corrosion [3]. The costs associated with controlling, reducing, and restoring corrosion, releasing toxic materials into the environment, and the subsequent effects on the biotic and abiotic components of the ecosystem are huge from an economic and environmental perspective [4]. Among the many anticorrosion methods, the anticorrosion coating is the most simple, effective, comprehensive, and economical [5]. Nowadays, conductive polymer coatings are widely used in various projects [6, 7].

Oxidative polymerization and electrochemical synthesis are two methods used to prepare conductive polymers, although other alternatives, such as photochemically initiated or enzyme-catalyzed polymerization, have also been observed [8-10]. In addition, galvanostatic, potentiostatic, and potentiodynamic electrochemical techniques can also be employed to synthesize electrically conductive polymers. Electrochemical synthesis has some benefits even though it can only produce a limited quantity of electrically conductive polymers. There is no requirement for an oxidizing agent because the electrochemical synthesis involves direct oxidation of the monomer at the

anode. On the other hand, in most cases, the polymer is deposited on an electrode, which facilitates further analysis. The electrochemical polymerization method affects aspects of the resulting polymers [11, 12].

The galvanostatic technique is the synthesis of electroconductive polymers under constant current density conditions. The polymer film obtained at the end of the polymerization is in a doped, i.e., conductive form [13-15]. The potentiostatic polymerization and potentiodynamic polymerization techniques use a constant positive potential and cyclic voltammetry, respectively.

The electrochemical synthesis of electroconductive polymers is typically carried out in a three-electrode cell setup, while galvanostatic synthesis can be carried out in a two-electrode system. In the three-electrode cell, the working electrode serves as an anode for polymerization and polymer deposition, the counter electrode is the point at which the electrolyte's solvent, dissolved oxygen, or other compounds are reduced, and the reference electrode controls the potential. The three electrodes may be arranged in one compartment (one compartment cell), two compartments (one for the counter and working electrodes and one for the reference electrode), three compartments (each electrode having its compartment), or any combination of these [16, 17].

Organic compounds containing heteroatoms such as oxygen, sulfur, or nitrogen atoms in their structures are often electropolymerized to produce effective polymeric coatings against corrosion. These compounds are selected based on their large molecular weight, functional polarity (such as -C=O, C=N), and extensive connections in aromatic rings, allowing them to adsorb on alloy surfaces [18]. There are many studies on the electropolymerization process to protect alloys from corrosion [19-23].

The aim of this study is to prepare polymeric coatings that protect the surface of Low-Carbon Steel (LCS) alloy from corrosion in a salt solution of 3.5% NaCl.

2. Experimental Work

The Low Carbon Steel (LCS) employed in this study has a chemical composition described in Table 1.

Table 1. Chemical components of LCS.

Alloy Type	**Chemical compositions (wt%)**								
	C	**Fe**	**Si**	**Mn**	**Cu**	**Ni**	**Cr**	**Mo**	**Others**
LCS	0.1	99.3	0.005	0.390	0.0315	0.022	0.0313	0.004	0.117

Initially, the LCS discs with a diameter of 25 mm, and a thickness of 15 mm were polished with silicon carbide emery paper of different grades (180, 220, 400, 1200, 2000, and 2500 mesh grit) and washed with tap water, distilled water, and then cleaned with acetone to remove grease and adhesives from the surface. Fig. 1 shows the LCS disks before and after polishing.

Electropolymerization of the monomer 6-((4 acetylphenyl)carbamoyl)cyclohex-3-ene-1-carboxylic acid (ACC) was performed on the surface of LCS disc using a DC power source and two electrodes: the working electrode (WE), the LCS disc, and the counter electrode (CE), a stainless steel plate. The coating solution for electropolymerization consisted of 0.1g (0.003 M) ACC monomer dissolved in 100 ml diluted ethanol with three drops of H_2SO_4 (98%). A voltage of 1.7 V was applied between the two electrodes at room temperature for 45 min. The coated electrode (LCS disc) was dried by a heat gun. Eq. (1) explains the synthesis of PACC polymer.

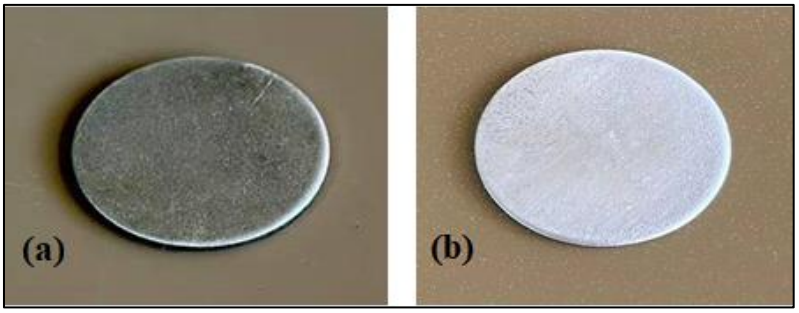

Figure 1: LCS discs a. before Polishing b. after polishing.

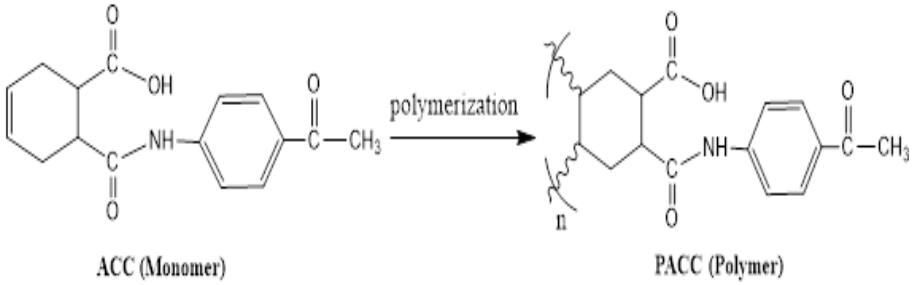

(1)

In addition, to enhancing the efficiency of the polymeric coating PACC against corrosion, it was added 40 or 50 ppm of nano zirconium dioxide (ZrO_2) and nano magnesium oxide (MgO), respectively to the coating solution to produce PACC-ZrO_2 nanocomposite and PACC-MgO nanocomposite [24].

Corrosion tests and measurements were performed using an electrochemical system containing a potentiostat\galvanostat device (WENKING M lab2000 Bank Electronic Intelligent Controls GmbH, Germany), a three-electrode corrosion cell, a thermostat, a magnetic stirrer, and a host computer (Fig. 2). The three-electrode corrosion cell (1-liter capacity) consists of internal and external bowls. Carbon steel was the working electrode, the platinum electrode with a length of 10 cm and diameter of 6 mm was an auxiliary electrode, and calomel was the reference electrode. The working electrode was immersed in the test solution (3.5% NaCl) for 15 minutes to establish a steady-state open circuit potential (E_{ocp}). The electrochemical measurements were carried out in a potential range of about ±200 mV. The tests were conducted at temperatures between 298 and 328 K, controlled via a water bath equipped with a thermostat [25-27]. Eq. (1) explains the synthesis of PACC polymer.

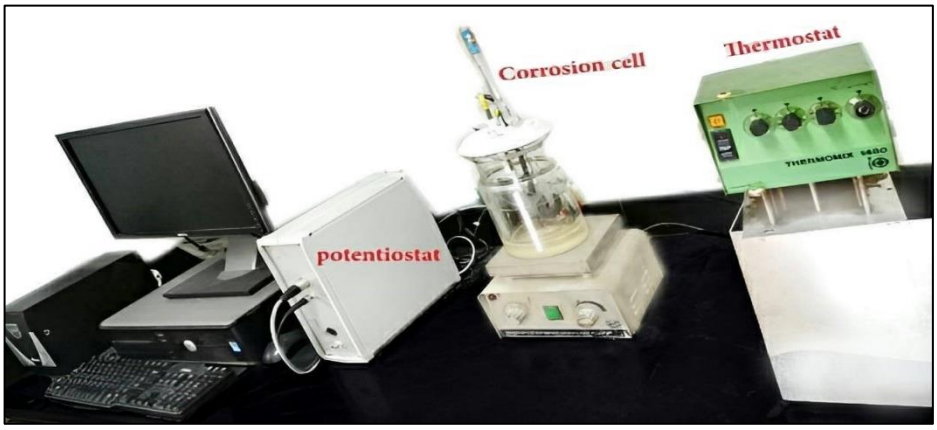

Figure 2: The system of polarization measurements.

3. Results and Discussions

3.1. The Suggested of ACC Polymerization on L.C.S Electrode

Based on previous studies [19-23], the mechanism of the ACC monomer electropolymerization on the LCS electrode surface has been suggested according to cationic electropolymerization, which takes place in the stages described below [28, 29]:

1. The working electrode accepts a single electron from the monomer molecule and a cationic radical is formed, as shown in steps 1 to 2 of Fig. 3.
2. This radical reacts with another monomer to form a dimer cationic radical.

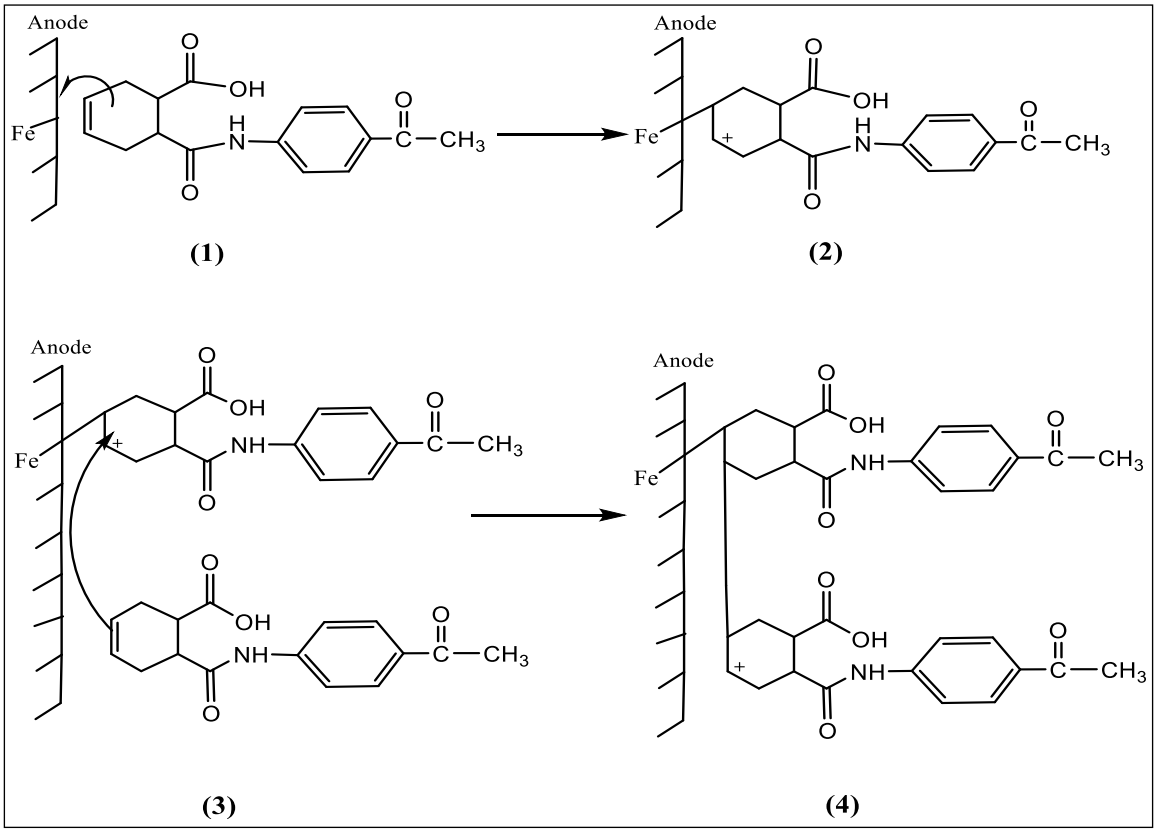

Figure 3: The Suggested Mechanism of ACC Electropolymerization on the LCS electrode.

3.2. Fourier transforms Infrared spectroscopy (FTIR) Analysis

Fourier transform Infrared spectroscopy (FTIR) analyzes the polymer (PACC) structure produced via electrochemical polymerization from the monomer (ACC). The FTIR spectrum of ACC monomer, (Fig. 4a), showed stretching bands at 3319 cm^{-1} for the NH amide group. The stretching bands at 3118 cm^{-1} are for the aromatic C-H and at 2925.81 and 2848 cm^{-1} for the aliphatic C-H. The acid, ketone, and amide carbonyl groups appeared at 1770, 1699.17, and 1677 cm^{-1}, respectively. Also, the olefinic =CH appeared at 3028 cm^{-1}. C=C bands appeared at 1595.02 cm^{-1}. The disappearance of the double bond (C=C) in Fig. 4b indicates that the polymer PACC has formed. The transmission peak is relatively broad because of the widespread PACC chain dispersion [30-32].

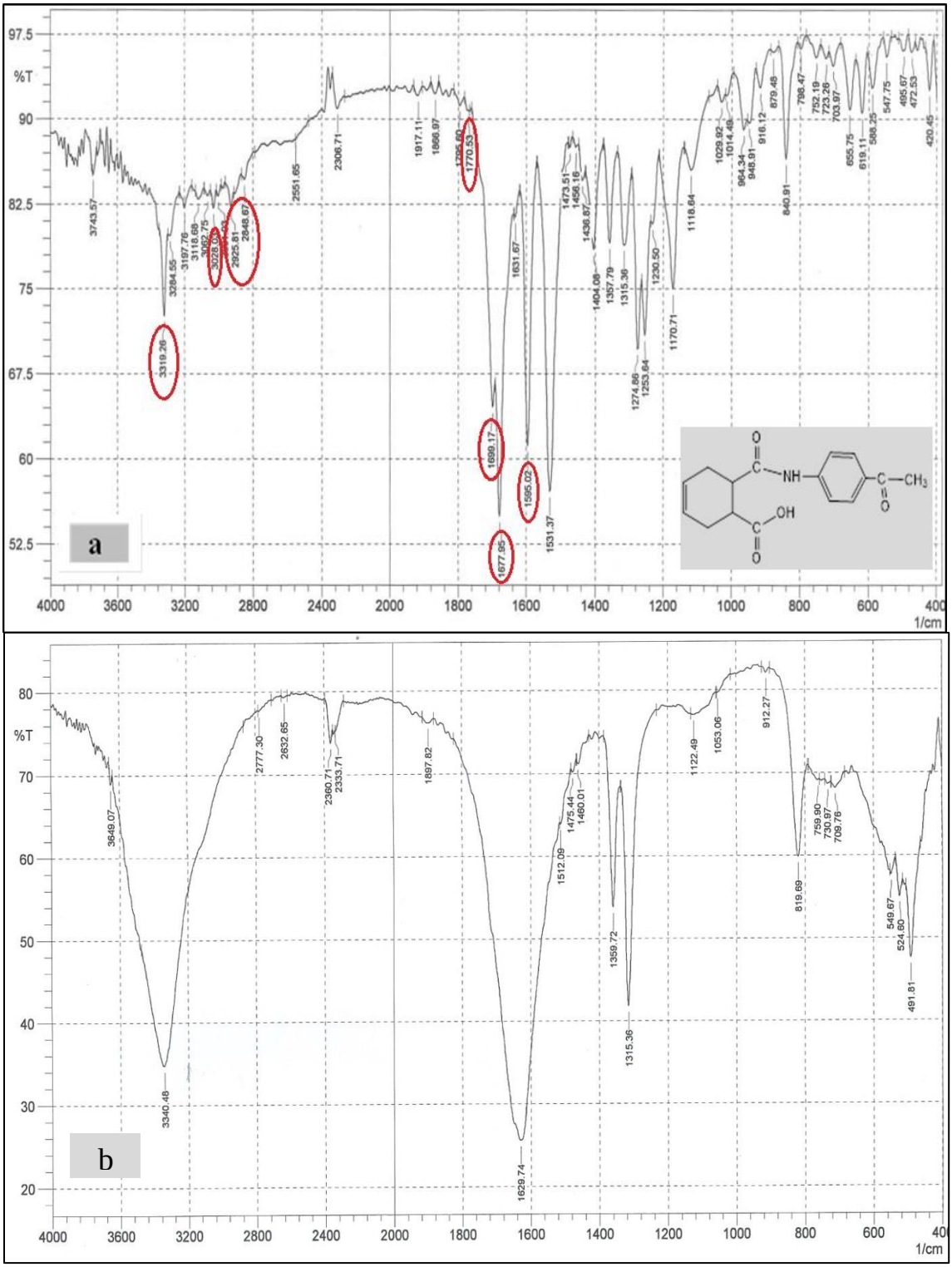

Figure 4: FTIR spectra of (a) ACC and (b) PACC.

3.3. Atomic Force Microscopy Analysis

The surface of LCS discs coated with PACC was topographically mapped using atomic force microscopy (AFM), both in the presence and absence of nanometal oxides. Fig. 5 (a, b, and c) shows three-dimensional images of the produced polymer with and without the nanometal oxides. The degree of the nanomaterial aggregation caused by ZrO_2 and MgO sticking to the polymer and creating smooth layers are shown in these images. Two of the parameters most often utilized in AFM analysis to describe the surface roughness of the prepared polymer films are average roughness (S_a) and root

mean square roughness (S_q). Table 2 lists the obtained S_a and S_q values for the LCS discs coated with PACC film with and without the nano metal oxides. The results indicate that, after the polymer was treated with the nano metal oxides, the surface roughness decreased (i.e., increase in smoothness) due to the reduction in grain size as a result of the nanomaterials interference within the polymer structure and the formation of polymer-nanocomposites [33, 34].

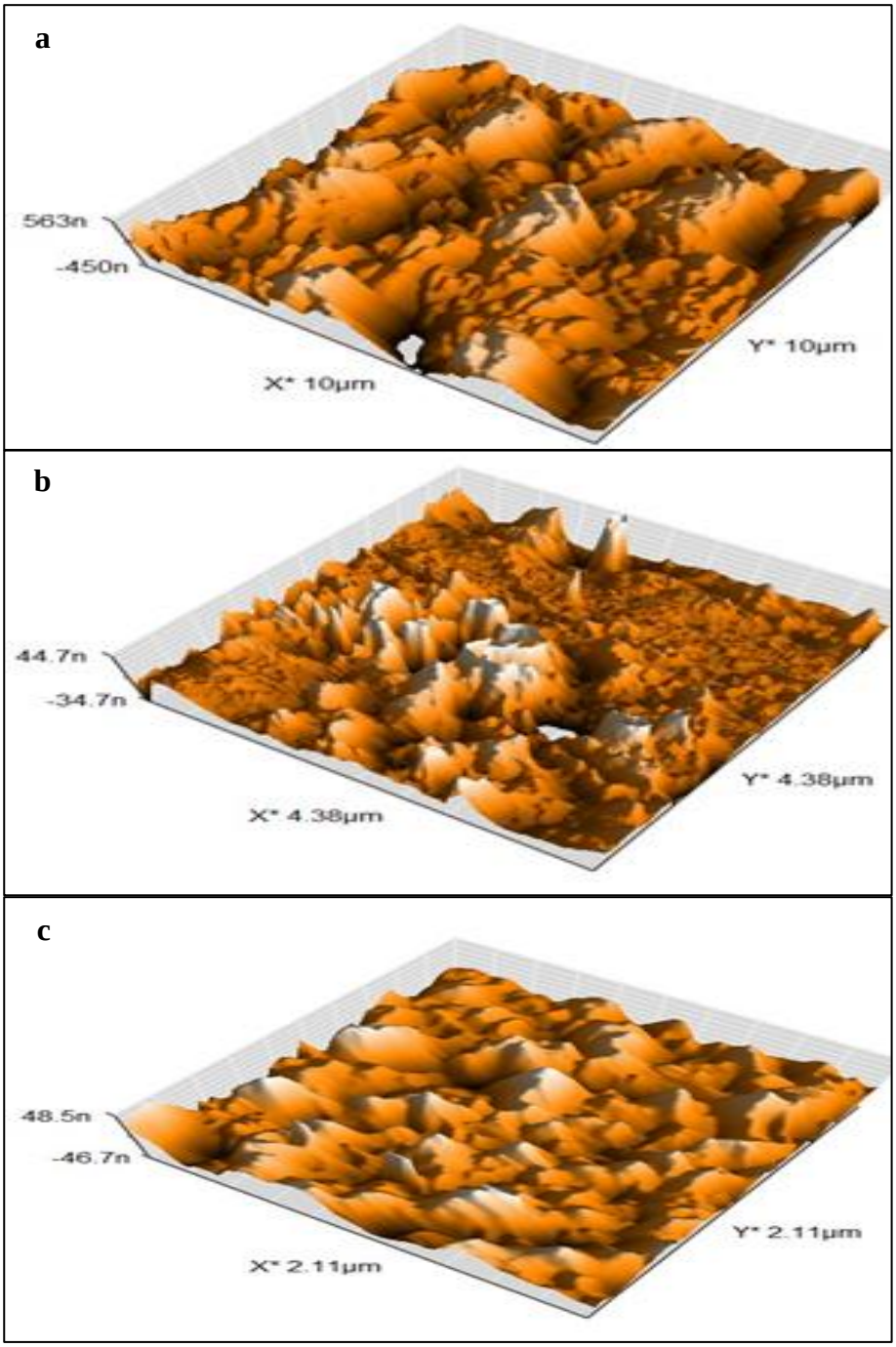

Figure 5: 3D AFM images of (a) LCS coated with PACC, (b) LCS coated with PACC-ZrO_2 nanocomposite, (c) LCS coated with PACC-MgO nanocomposite.

Table 2. AFM parameters for LCS disc coated with PACC film with and without the nano metal oxides.

System	S_a (nm)	S_q (nm)	Main grain size (nm)
PACC	149.9	197.2	165.4
PACC-ZrO_2 nanocomposite	32.15	40.64	83.78
PACC-MgO nanocomposite	60.95	77.67	66.16

3.4. Corrosion Tests

The kinetics of the anodic and cathodic reactions was studied through polarization measurements. Carbon steel's polarization curves in a 3.5% NaCl solution with and without PACC and PACC-metal oxides nanocomposite at temperatures ranging from 298 to 328 K are displayed in Fig. 6. The corrosion current density (i_{corr}) and corrosion potential (E_{corr}) were achieved at the intersection of the anodic and cathodic current-potential curves. The electrochemical characteristics for the LCS disc in 3.5% NaCl solution with and without PACC and PACC-metal oxides nanocomposite are shown in Table 3 by Tafel plots (i_{corr}, E_{corr}, C.R, PL, β_a, and β_c) [35]. Equation (2) was used to calculate the protection efficiency, PE% (included in Table 3), using the i_{corr} values [36]:

$$PE\% = \frac{i_{corr,uncoated} - i_{corr,coated}}{i_{corr,uncoated}} \times 100 \quad (\mathbf{2})$$

where: $i_{corr,coated}$ and $i_{corr,uncoated}$ are the corrosion current densities for the coated and uncoated LCS discs, respectively. The Stern-Gery equation (Eq. (3)) was used to compute the polarization resistance (R_p) (listed in Table 3) [37, 38]:

$$R_p \frac{\beta_a|\beta_c|}{2.303(\beta B_a + |\beta_c|)i_{corr}} \quad (\mathbf{3})$$

where: βa and βc are anodic and cathodic tafel slopes, respectively and i_{corr} is corrosion current density.

3.5. Activation Parameters of Corrosion: Kinetic and Thermodynamic

The effect of temperatures on the rate of corrosion of the LCS disc in the absence and presence of various coatings of (PACC) was investigated at temperatures between 298 and 328 K. To determine the activation parameters of the corrosion process, the Arrhenius Eqs. 4 and 5 were applied for the activated complex created during the transition state [38, 39]. The outcomes are shown in Table 4 and Figs. 7 and 8.

$$\log C.R = \log A - \frac{E_a}{2.303\ RT} \quad (\mathbf{4})$$

$$\log \frac{C.R}{T} = \log\left(\frac{R}{Nh}\right) + \frac{\Delta S^*}{2.303\ R} - \frac{\Delta H^*}{2.303RT} \quad (\mathbf{5})$$

where: A is the Arrhenius preexponential factor, T is the absolute temperature (K), R is the molar gas constant ($JK^{-1}mol^{-1}$), E_a is the apparent effective activation energy, C.R is the corrosion rate, which is equal to the corrosion current density, N is Avogadro's number, and h is the Planck constant.

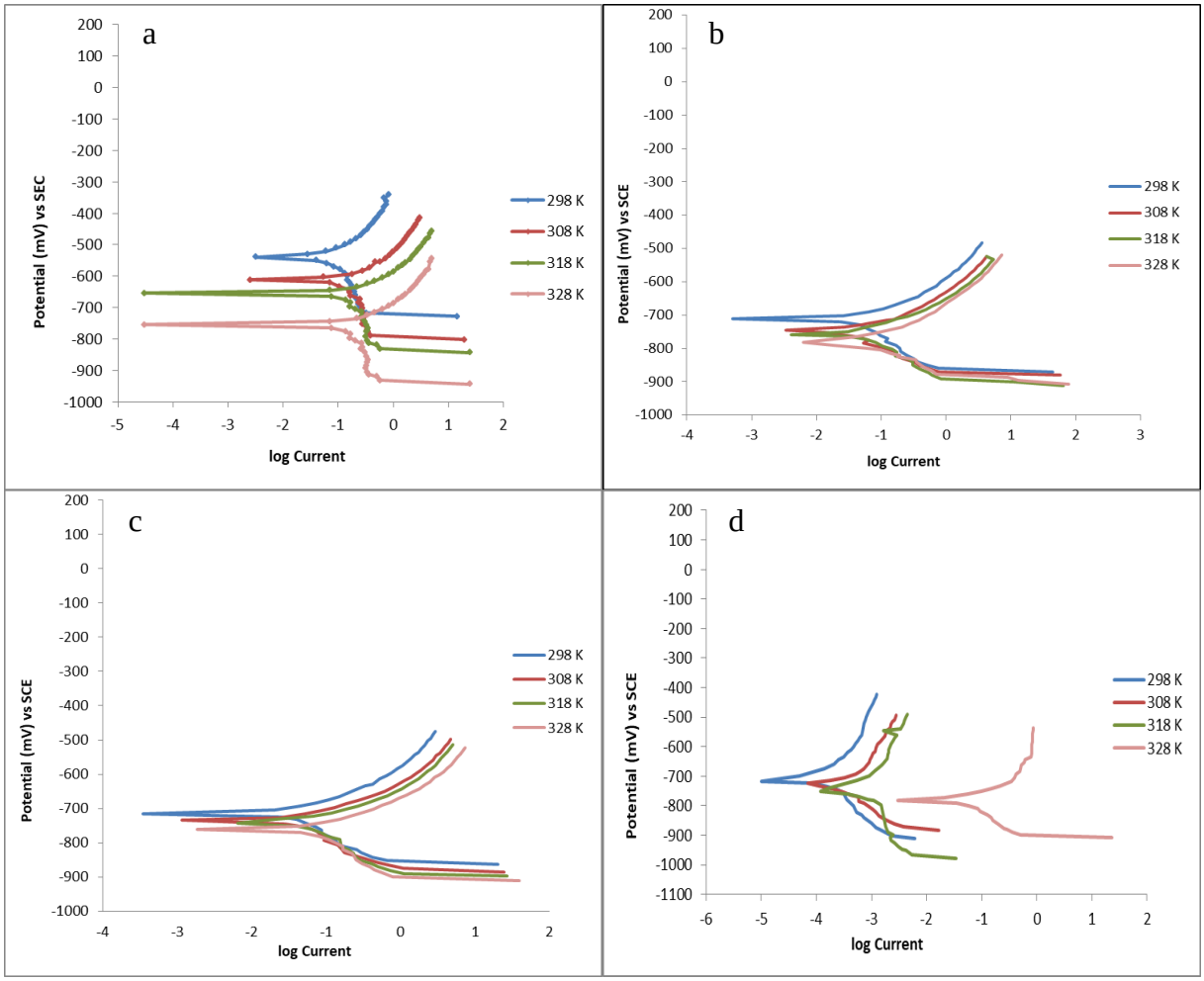

Figure 6: Polarization diagrams for the (a) uncoated LCS disc, (b) LCS disc coated with PACC, (c) LCS disc coated with PACC-ZrO_2 nanocomposite and (d) LCS disc coated with PACC–MgO nanocomposite.

Table 3: Corrosion parameters for LCS discs in a 3.5% NaCl solution at different temperatures.

System	T (K)	E_{corr} (mV)	i_{corr} (μA/cm^2)	βc (mV/Dec)	βa (mV/Dec)	CR (mm/y)	PL (g/m^2.d)	PE%	R_p (Ω/cm^2)
Uncoated LCS	298	-530.0	63.51	-142.1	104.8	1.59	0.737	-	412.38
	308	-610.0	76.20	-145.1	120	1.90	0.885	-	374.27
	318	-650.0	117.69	-239.4	80.1	2.94	1.370	-	221.43
	328	-691.1	141.82	-449.6	70.9	3.55	1.650	-	187.50
LCS coated with PACC	298	-712	14.27	-79.8	60.6	0.35	0.166	77.5	1048
	308	-745	18.67	-72	75.3	0.46	0.217	75.4	856
	318	-759	29.33	-81.4	75	0.73	0.340	75.0	577
	328	-781	37.73	-88.4	63.1	0.94	0.438	73.3	423
LCS coated with PACC +ZrO_2 Nanocomposite	298	-714.7	9.51	-62.3	50.2	0.23	0.110	85.0	1269
	308	-732.5	12.93	-71.6	60.6	0.32	0.150	83.0	1102
	318	-742.8	22.95	-75.9	69.9	0.57	0.266	80.4	688
	328	-763	28.85	-86.4	68.1	0.72	0.335	79.6	573
LCS coated with PACC +MgO Nanocomposite	298	-717.8	0.13	-143.8	131.8	0.03	0.152	99.7	227614
	308	-724.3	0.40	-255.5	325.5	0.26	0.173	99.4	155222
	318	-750.1	1.06	-279.7	210.9	0.29	0.265	99.0	49254
	328	-782.8	11.33	84.9	83.3	0.38	0.432	92.0	1611

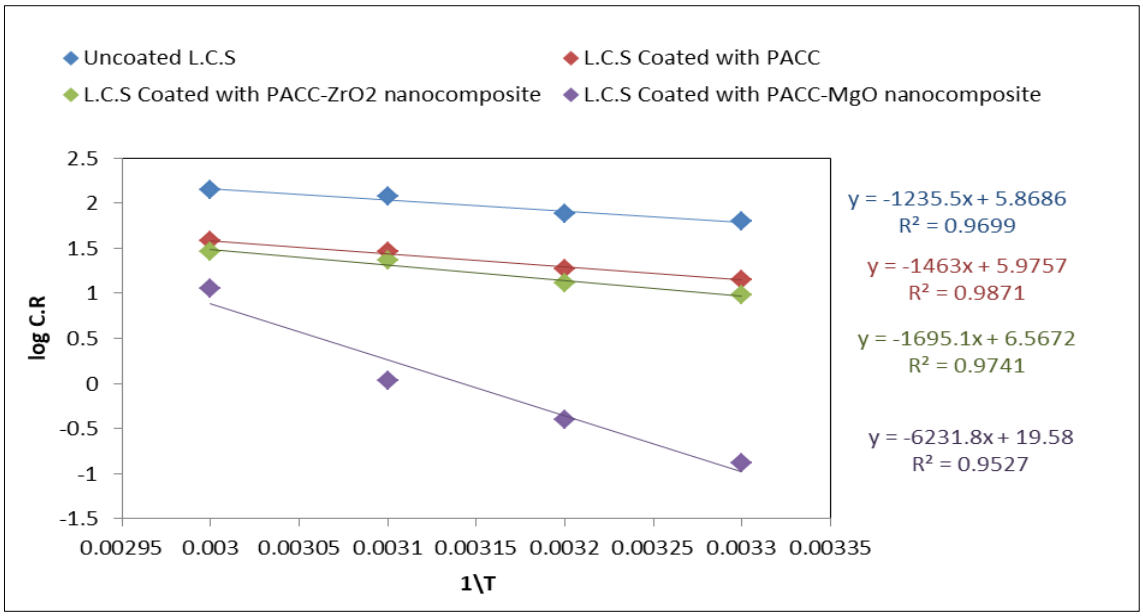

Figure 7: The relationship between log C.R and 1\T of LCS disc uncoated and coated with PACC with and without nano oxides in a solution of (3.5% NaCl).

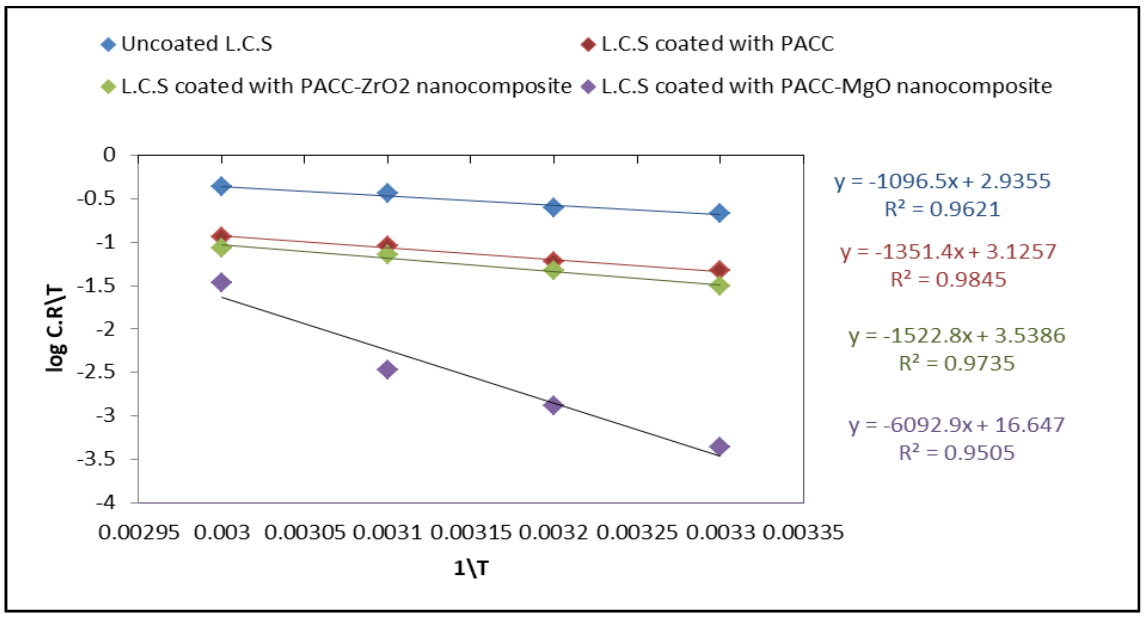

Figure 8: The relationship between log (C.R\T) and (1\T) of LCS disc uncoated and coated with PACC with and without nano oxides in a solution of (3.5% NaCl).

Table 4: Kinetic and thermodynamic activation parameters for LCS discs uncoated and coated with PACC with and without nano oxides at various temperatures.

System	E_a^* (kJ\mol)	A (Molecule .cm^{-2}. S^{-1})	ΔH^* (kJ\mol)	ΔS^* (J/mol. K)
Uncoated L.C. S	23.656	4.448×10^{29}	20.994	-141.373
LCS coated with PACC	28.012	5.692×10^{29}	25.875	-137.731
LCS coated with PACC-ZrO_2 nanocomposite	32.456	2.222×10^{30}	29.157	-129.826
LCS coated with PACC-MgO nanocomposite	119.321	2.288×10^{43}	166.661	121.162

The results showed that the thermodynamic activation parameters values (Ea* and H*) for PACC and PACC metal oxide nanocomposites coated LCS discs are greater than those for uncoated LCS discs. This suggests that the energy barrier has risen. The entropy of activation values for polymeric-coated and uncoated LCS discs are negative and increase to be positive, showing that the activated complex in the rate-determining step was achieved in an association rather than a dissociation step. Additionally, there was less disordering when transitioning from reactants to activated complexes [40, 41].

4. Electrochemical Impedance Spectroscopy

The behavior of a corroding alloy to small-amplitude alternating potential signals of widely variable frequency was studied using Electrochemical Impedance Spectroscopy (EIS). It was analyzed by Nyquist plots when the imaginary part of the impedance was plotted as a function of its real part. The Bode plot shows the phase angle (Θ) and the total impedance |Z|. The Nyquist plot yielded the impedance parameters, capacitance, and polarization resistance (R_p). The following equation shows the uncompensated resistance (R_s) between the working and reference electrodes and the capacitance (C_c) of the polymer film [42, 43]:

$$C_C = \varepsilon\varepsilon_\circ \frac{A}{d} \qquad (6)$$

where: $\varepsilon_\circ$is the dielectric constant in free space (8.85×10^{-12} A/cm), ε is the dielectric constant for the polymer, d is the thickness of the film, and A is the exposed area of alloy.

The experimental results of EIS for the LCS discs uncoated and coated with PACC in 3.5% NaCl solution were represented by Nyquist plots and Bode plots, as shown in Figs. 9-11.

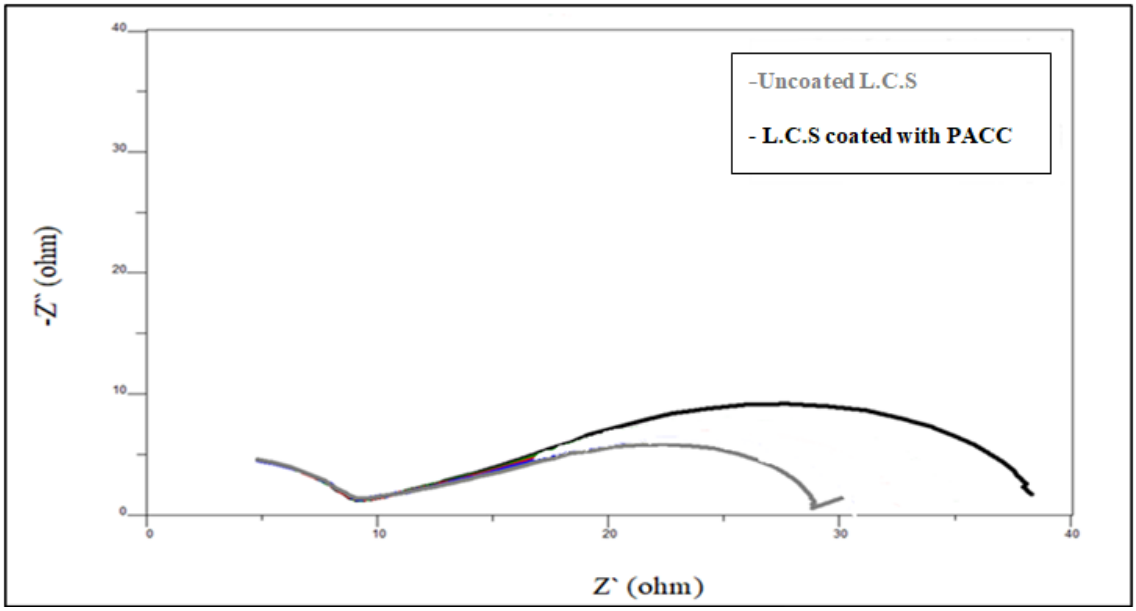

Figure 9: Nyquist plots for LCS uncoated and coated with PACC in 3.5% NaCl solution.

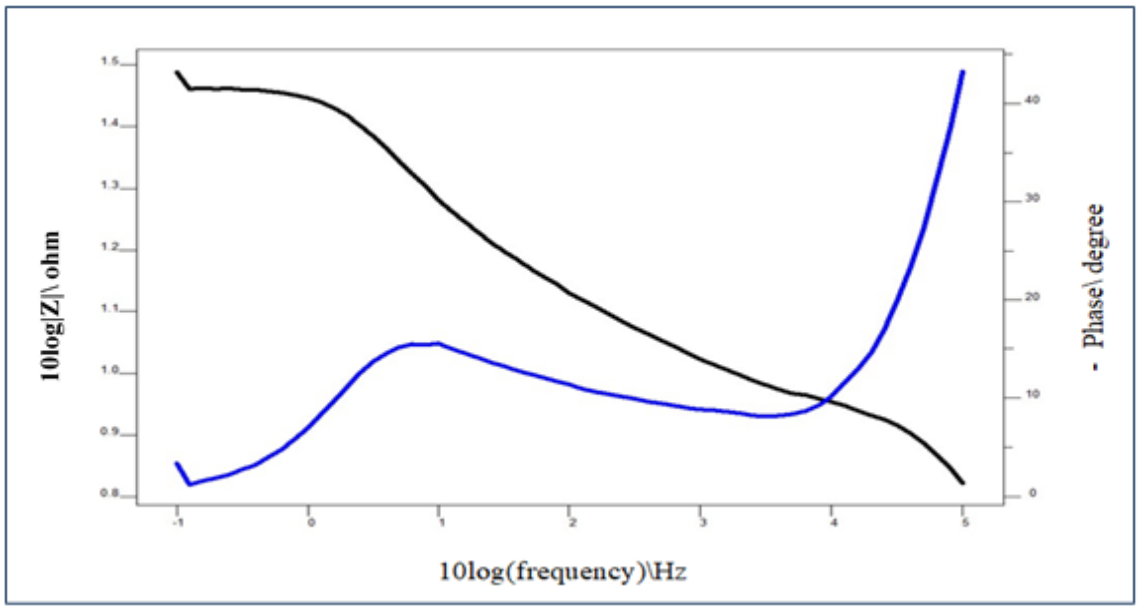

Figure 10: Bode plots for uncoated LCS discs in 3.5% NaCl solution.

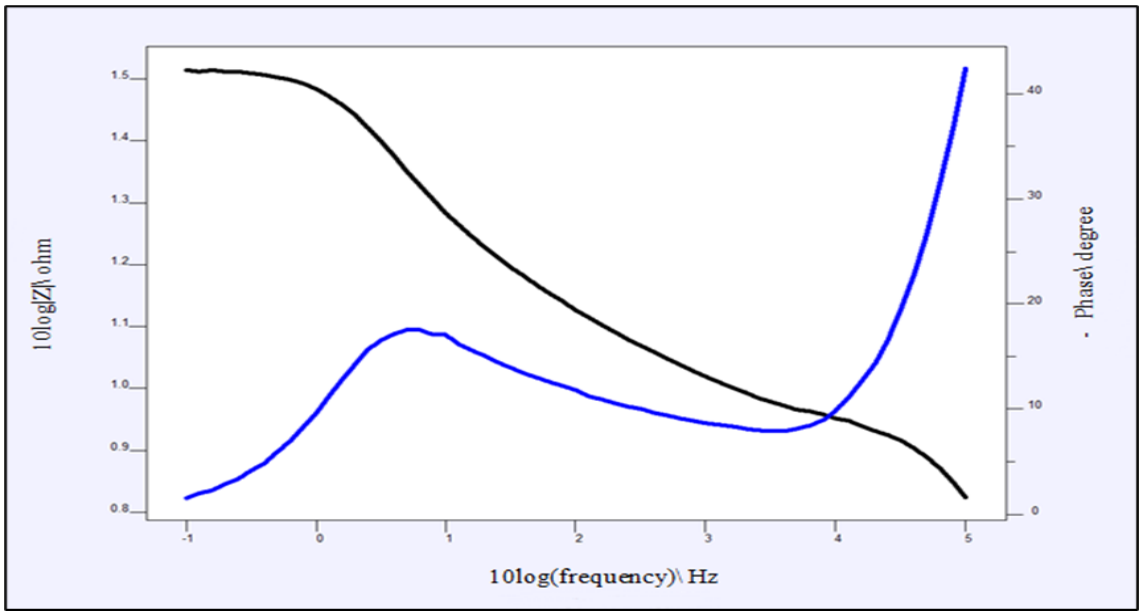

Figure 11: Bode plots for LCS discs coated with PACC in 3.5% NaCl solution.

The EIS spectrum was referred to as coating behavior in the high-frequency area and corrosion reaction in the low-frequency zone [44, 45].

According to the Nyquist plots and impedance values (ź), the corrosion resistance of the uncoated LCS discs was lower than that of the coated discs because the polymer films inhibit the penetration of ions and water into the coating and the subsequent electrochemical reactions at the coating/metal interface, leading to the improvement of the barrier performance of the polymer coating [46, 47]. This demonstrates the coating's effectiveness in protecting the LCS discs surface against corrosion.

The electrochemical equivalent circuits of the uncoated and coated LCS discs were obtained from the best fit to the impedance data for the uncoated and coated LCS discs in 3.5% NaCl solution at room temperature. They had the same equivalent circuit, as shown in Fig. 12.

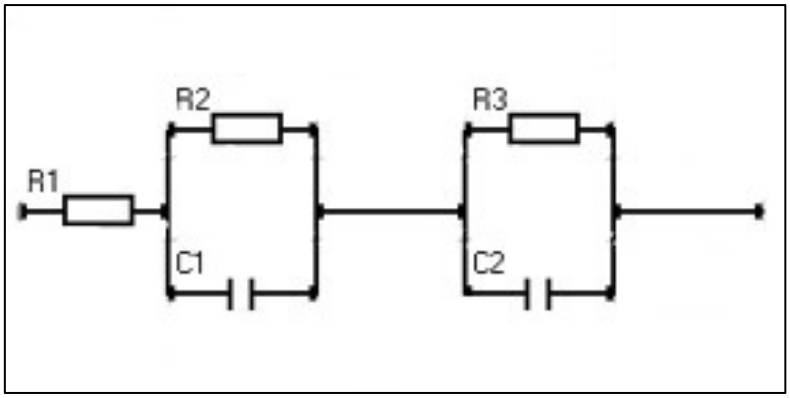

Figure 12: The equivalent circuit of the uncoated and coated LCS discs.

The electrochemical parameters obtained from the equivalent circuit are [48]:

- R_1 = electrolyte resistance
- R_2 = pore resistance
- R_3= charge transfer resistance
- C_1 = coating capacitance
- C_2 = double layer capacitance

These parameters values are listed in Table 4-9.

Table 5: Electrochemical parameters of the equivalent circuit for the LCS discs uncoated and coated with PACC polymer.

System	R_1 (Ω)	R_2 (Ω)	R_3 (Ω)	C_1 (F)	C_2 (F)
Uncoated LCS	7.987	1.072	2.988	2.147×10^{-3}	0.912×10^{-4}
LCS coated with PACC	8.823	1.838	7.633	3.527×10^{-3}	1.434×10^{-4}

The values of R_1, R_2 and R_3 for the LCS discs coated with the polymer were higher than that of the uncoated LCS discs and that referred to the increased resistance against corrosion [49, 50].

5. Conclusion

The results indicated the following conclusions:

- The prepared polymeric films (PACC) provided good protection for LCS alloy surface against corrosion in a solution of 3.5%NaCl. The efficiency of this protection decreased with increasing temperature.
- The protection efficiency of the prepared polymeric films against LCS corrosion of 77.5% at 298 K increased to 85.0% and 99.7 by adding the nanomaterial oxides of ZrO_2 and MgO, respectively.
- The kinetic and thermodynamic studies showed that the activation energies of LCS corrosion increased after coating due to the increase of the energy barrier for the corrosion process.
- The polarization resistance of the alloy increased after coating, as indicated by the measurements potentiostat and EIS.

Acknowledgement

The authors of this article extend their sincere thanks to the presidency and staff of the Chemistry Department in the College of Science, University of Baghdad for the facilities they provided to complete this work.

Conflict of interest

Authors declare that they have no conflict of interest

References

1. P. R. Ammal, M. Prajila, and A. Joseph, J. Envir. Chem. Eng. **6**, 1072 (2018).
2. V. Vorobyova, M. Skiba, and E. Gnatko, S. African J. Chem. Eng. **43**, 273 (2023).
3. A. Tenorio-Alfonso, M. C. Sánchez, and J. M. Franco, J. Poly. Envir. **28**, 749 (2020).
4. M. A. Bedair, H. M. Elaryian, E. S. Gad, M. Alshareef, A. H. Bedair, R. M. Aboushahba, and A. E.-a. S. Fouda, RSC Advances **13**, 478 (2023).
5. S. De and J. L. Lutkenhaus, Gre. Chem. **20**, 506 (2018).
6. R. Mohammed and K. Saleh, Eurasian Chem. Commun. **3**, 715 (2021).
7. S. A. Umoren and M. M. Solomon, Prog. Mater. Sci. **104**, 380 (2019).
8. S. Cherdchom, W. Keawsongsaeng, W. Buasorn, N. Rimsueb, P. Pienpinijtham, A. Sereemaspun, R. Rojanathanes, and P. Aramwit, ACS Omega **6**, 28880 (2021).
9. S. Bhadra, D. Khastgir, N. K. Singha, and J. H. Lee, Prog. Poly. Sci. **34**, 783 (2009).
10. U. Saviour, Prog. Mat. Sci. **104**, 380 (2019).
11. B. D. Malhotra, *Handbook of Polymers in Electronics* (UK, Rapra Technology Limited, 2001).
12. Y. Samet, D. Kraiem, and R. Abdelhédi, Prog. Org. Coat. **69**, 335 (2010).
13. J. Heinze, B. A. Frontana-Uribe, and S. Ludwigs, Chem. Rev. **110**, 4724 (2010).
14. M. I. Khan, A. U. Chaudhry, S. Hashim, M. K. Zahoor, and M. Z. Iqbal, Chem. Eng. Res. Bull. **14**, 73 (2010).
15. S. El Aggadi, N. Loudiyi, A. Chadil, Z. El Abbassi, and A. El Hourch, Mediterran. J. Chem. **10**, 138 (2020).
16. M. M. Gvozdenović, B. Jugović, J. Stevanović, and B. N. Grgur, Hemij. Indust. **68**, 673 (2014).
17. Y. Jiang, W. Zheng, K. Tran, E. Kamilar, J. Bariwal, H. Ma, and H. Liang, Nat. Commun. **13**, 197 (2022).
18. N. A. Khudhair, A. T. Bader, M. I. Ali, and M. Husseini, AIP Conference Proceedings (Karbala, Iraq AIP Publishing, 2020). p. 030014.
19. R. A. Mohammed and K. A. Saleh, Chem. Methodol. **6**, 74 (2022).
20. M. I. Ali and K. A. Saleh, IOP Conference Series: Materials Science and Engineering (IOP Publishing, 2019). p. 012072.
21. R. A. Mohammed and K. A. Saleh, Mater. Today Proce. **61**, 805 (2022).
22. A. Khulood, S. Khalil, and I. Muna, J. Phar. Bio. Sci. **13**, 30 (2018).
23. W. S. Hummers, Jr. and R. E. Offeman, J. American Chem. Soci. **80**, 1339 (1958).
24. A. M. Alqudsi and K. A. Saleh, Baghdad Sci. J. **21**, 1243 (2024).
25. Z. Hussain and K. A Saleh, J. Nanostruc. **13**, 718 (2023).
26. I. M. Mohammed, Baghdad Sci. J. **16**, 0049 (2019).
27. R. L. Shriner, R. Fuson, and D. Y. Curtin, *Thesystematic identification of organic compounds* (Canada, John Wileyand Sons, Inc, 1948).
28. K. S. Khalil, K. A. Saleh, and M. I. Khalaf, Int. J. Pharma. Qual. Ass. **9**, 253 (2018).
29. Y. Zhao, Z. Wei, Q. Pang, Y. Wei, Y. Cai, Q. Fu, F. Du, A. Sarapulova, H. Ehrenberg, and B. Liu, ACS Appl. Mater. Inter. **9**, 4709 (2017).
30. K. G. Alves, J. F. Felix, E. F. De Melo, C. G. Dos Santos, C. A. Andrade, and C. P. De Melo, J. Appl. Poly. Sci. **125**, E141 (2012).
31. H. A. Al-Mashhadani and K. A. Saleh, Res. J. Pharm. Tech. **13**, 4687 (2020).

32. R. M. Kubba, M. A. Mohammed, and L. S. Ahamed, Baghdad Sci. J. **18**, 0113 (2021).
33. S. A. Alkhfaji and M. I. Ali, Ibn AL-Haitham J. Pure Appl. Sci. **35**, 161 (2022).
34. M. Molaei, A. Fattah-Alhosseini, M. Nouri, P. Mahmoodi, S. H. Navard, and A. Nourian, Surf. Inter. **30**, 101967 (2022).
35. R. A. Mohammed and K. A. Saleh, Iraqi J. Sci. **63**, 4163 (2022).
36. K. A. Saleh and M. I. Ali, Iraqi J. Sci. **61**, 1 (2020).
37. M. I.Ali and K. A.Saleh, Int. J. Eng. Tech. **7**, 5821 (2018).
38. K. a. K. Al-Rudaini and K. a. S. Al-Saadie, Iraqi J. Sci. **62**, 363 (2021).
39. M. Husaini, B. Usman, and M. B. Ibrahim, Bayero J. Pure Appl. Sci. **11**, 88 (2018).
40. G. K. Gomma and M. H. Wahdan, Mater. Chem. Phys. **39**, 209 (1995).
41. A. J. Huh and Y. J. Kwon, J. Cont. Rel. **156**, 128 (2011).
42. S. A. Umoren, M. J. Banera, T. Alonso-Garcia, C. A. Gervasi, and M. V. Mirífico, Cellulose **20**, 2529 (2013).
43. M. Hosseini, L. Fotouhi, A. Ehsani, and M. Naseri, J. Coll. Inter. Sci. **505**, 213 (2017).
44. A. U. Ammar, M. Shahid, M. K. Ahmed, M. Khan, A. Khalid, and Z. A. Khan, Materials **11**, 332 (2018).
45. T. Ohtsuka, A. Nishikata, M. Sakairi, and K. Fushimi, *Electrochemistry for Corrosion Fundamentals* (Japan, Springer, 2018).
46. A. Farhan and N. Kadhim, PhD. Thesis, University of Baghdad, 2018.
47. B. Javanpour, M. Azadbeh, and M. Mozammel, J. Inorg. Organomet. Poly. Mater. **30**, 4082 (2020).
48. E. Locorotondc, L. Pugi, L. Berzi, M. Pierini, S. Scavuzzc, A. Ferraris, A. G. Airale, and M. Carello, 2019 IEEE 5th International forum on Research and Technology for Society and Industry (RTSI) (Florence, Italy IEEE, 2019). p. 225.
49. M. Deyab, K. Eddahaoui, R. Essehli, S. Benmokhtar, T. Rhadfi, A. De Riccardis, and G. Mele, J. Molec. Liq. **216**, 699 (2016).
50. Ł. Drewniak and S. Kochowski, J. Mater. Sci. Mater. Elec. **31**, 19106 (2020).

دراسة أداء الحماية من التآكل لبوليمر والمتراكبات النانوية للبوليمر مع اكاسيد المعادن PACC المتبلمرة كهربائيا على سطح الفولاذ منخفض الكربون

زينب حسين[1] وخلود عبد صالح[1]

[1] قسم الكيمياء، كلية العلوم، جامعة بغداد، بغداد، العراق.

الخلاصة

في الدراسة الحالية، تم تحضير بوليمر جديد وهو poly 6-((4 acetylphenyl)carbamoyl)cyclohex-3-ene-1-) (carboxylic acid (PACC) ببلمرة مونومر of 6-((4 acetylphenyl)carbamoyl)cyclohex-3-ene-1-carboxylic acid (ACC) باستخدام عملية البلمرة الكهربائية, والبوليمر الناتج تم تشخيصه باستخدام مطيافية الاشعة تحت الحمراء . تمت دراسة قدرة هذا البوليمر على حماية السبيكة من التآكل عند درجات حرارة تتراوح بين 298 و328 كلفن. تم تقييم قدرة هذه الطلاءات على منع التآكل من خلال قياس تيار التآكل وجهد التآكل باستخدام جهاز قياس الجهد. لقد تم تعزيز كفاءة هذه الطلاءات البوليمرية بإضافة اكاسيد المعادن النانوية وهي اوكسيد الزركونيوم واوكسيد المغنيسيوم. كانت كفاءة الحماية للبوليمر وحده 77.5, زادت هذه الكفاءة إلى 85.0٪ و99.7٪ في وجود اوكسيد الزركونيوم النانوي واوكسيد المغنيسيوم النانوي على التوالي، لقد تم حساب المعلمات الحركية والثرموداينمكية للفولاذ منخفض الكربون المطلي وغير المطلي. كما تم دراسة مورفولوجية سطح الطلاء باستخدام مجهر القوة الذرية. وكذلك تم قياس المقاومة المعاقة باستخدام تقنية التحليل الطيفي للمقاومة الكهروكيميائية.

الكلمات المفتاحية: الحماية من التآكل، البوليمرات الموصلة، البلمرة الكهربائية، PACC، تافل.